

AD-A099 475 AEROSPACE CORP. EL SEGUNDO CA SPACE SCIENCES LAB
ANALYSIS OF A SERIES OF SOLAR FLARE X-RAY SPECTRA. (U)
MAY 81 D L MCKENZIE, P B LANDECKER
UNCLASSIFIED TR-0081(6900-01)-5

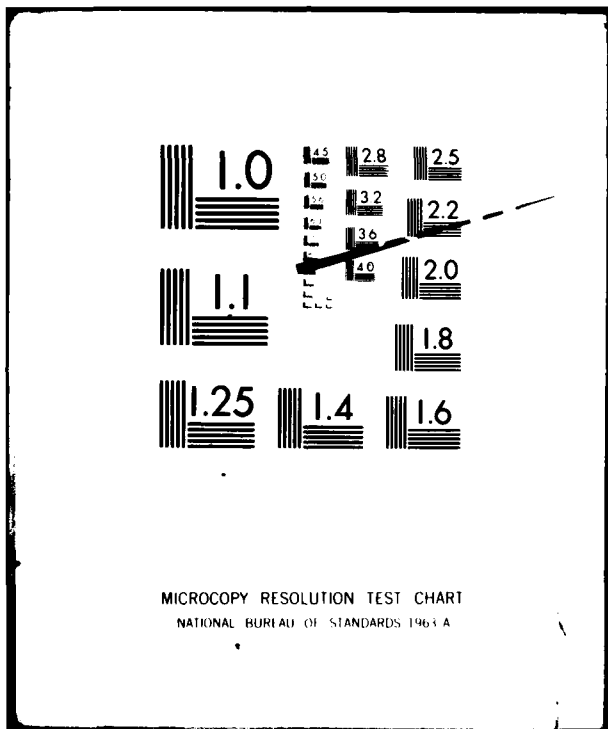
P/0 3/2

F04701-80-C-0081

SD-TR-81-91

ML

END
DATE
6 81
DTIC



DTIC FILE NUMBER

ADA 099475

LEVEL I

12
S.S.

Analysis of a Series of Solar Flare X-Ray Spectra

D. L. MURKIN and P. B. LANDIS
National Bureau of Standards
National Bureau of Standards
U.S. Air Force Command
Washington, D.C. 20234

1 May 1981

DTIC
ELECTRONIC
S
MAY 29 1981
D

Prepared for
SPACE DIVISION
AIR FORCE SYSTEMS COMMAND
Los Angeles Air Force Station
P.O. Box 92960, Worldway Postal Center
Los Angeles, Calif. 90009

815 29 049

This report was submitted by The Aerospace Corporation, El Segundo, CA 90245, under Contract No. F04701-80-C-0081 with the Space Division, Deputy for Technology, P.O. Box 92960, Worldway Postal Center, Los Angeles, CA 90009. It was reviewed and approved for The Aerospace Corporation by G. A. Paulikas, Director, Space Sciences Laboratory. Lt. Randall S. Weidenheimer, SD/YLVS, was the Project Officer for Mission-Oriented Investigation and Experimentation (MOIE) Programs.

This report has been reviewed by the Public Affairs Office (PAS) and is releasable to the National Technical Information Service (NTIS). At NTIS, it will be available to the general public, including foreign nations.

This technical report has been reviewed and is approved for publication. Publication of this report does not constitute Air Force approval of the report's findings or conclusions. It is published only for the exchange and stimulation of ideas.

Randall S. Weidenheimer
Randall S. Weidenheimer, 2nd Lt, USAF
Project Officer

Florian P. Meinhardt
Florian P. Meinhardt, Lt Col, USAF
Director of Advanced Space Development

FOR THE COMMANDER

William Goldberg
William Goldberg, Colonel, USAF
Deputy for Technology

UNCLASSIFIED

SECURITY CLASSIFICATION OF THIS PAGE (When Data Entered)

19 REPORT DOCUMENTATION PAGE		READ INSTRUCTIONS BEFORE COMPLETING FORM
1. REPORT NUMBER SD-TR-81-41	2. GOVT ACCESSION NO. AD-A099 475	3. RECIPIENT'S CATALOG NUMBER
4. TITLE (and Subtitle) ANALYSIS OF A SERIES OF SOLAR FLARE X-RAY SPECTRA	5. TYPE OF REPORT & PERIOD COVERED Technical Report 1 Jan 1981 - 31 Dec 1981	
6. AUTHOR(s) D. L. McKenzie P. B. Landecker	7. PERFORMING ORGANIZATION NAME AND ADDRESS The Aerospace Corporation El Segundo, Calif. 90245	
8. CONTRACT OR GRANT NUMBER(s) F04701-80-C-0081	9. PROGRAM ELEMENT, PROJECT, TASK AREA & WORK UNIT NUMBERS 15	
10. CONTROLLING OFFICE NAME AND ADDRESS Space Division Air Force Systems Command Los Angeles, Calif. 90009	11. REPORT DATE 1 May 81	
12. MONITORING AGENCY NAME & ADDRESS (if different from Controlling Office)	13. NUMBER OF PAGES 40	
	14. SECURITY CLASS. (of this report) Unclassified	
	15a. DECLASSIFICATION/DOWNGRADING SCHEDULE	
16. DISTRIBUTION STATEMENT (of this Report) Approved for public release; distribution unlimited		
17. DISTRIBUTION STATEMENT (of the abstract entered in Block 20, if different from Report)		
18. SUPPLEMENTARY NOTES		
19. KEY WORDS (Continue on reverse side if necessary and identify by block number) Solar Corona Solar Flares X-ray Spectra		
20. ABSTRACT (Continue on reverse side if necessary and identify by block number) We analyze thirteen X-ray line spectra (7.8-23.0 Å) acquired during a solar flare that peaked at 2326 UT on 1979 March 31. The data include fluxes of lines excited throughout the temperature range $2-18 \times 10^6$ K, the entire range present in the coronal flare. The coronal flare emission measure began to decrease 500 s or less after the broad band X-ray flux peaked. We construct the differential emission measure $\epsilon(T)$ for $2-18 \times 10^6$ K from the data by using collision strengths now available for a small number of the observed lines.		

UNCLASSIFIED

SECURITY CLASSIFICATION OF THIS PAGE(When Data Entered)

19. KEY WORDS (Continued)

20. ABSTRACT (Continued)

The total emission measure for T greater than $2 \times 10^6 K$, the radiative energy loss rate, the density at $2 \times 10^6 K$, and the conductive cooling time are derived from the data, but lack of information on electron densities prevents a detailed study of the flare energetics. This situation is unlikely to improve in the near future. Conductive cooling was more important than radiative cooling for coronal temperatures in this flare.

UNCLASSIFIED

SECURITY CLASSIFICATION OF THIS PAGE(When Data Entered)

PREFACE

D. K. Watson, G. A. Doschek, and U. Feldman provided helpful discussions. S. H. Painter aided in the data reduction.

Accession For	
NTIS GRA&I	<input checked="" type="checkbox"/>
DTIC TAB	<input type="checkbox"/>
Unannounced	<input type="checkbox"/>
Justification	
By _____	
Distribution/ _____	
Availability Codes	
Dist	Avail and/or Special
A	

CONTENTS

PREFACE.....	1
I. INTRODUCTION.....	9
II. THE FLARE DATA.....	10
III. ANALYSIS.....	13
IV. SUMMARY.....	34
REFERENCES.....	36

FIGURES

1. Dead Time Corrected Profiles of Selected X-Ray Lines
Observed During the 1979 March 31 Flare..... 12
2. The Line Flux of Selected Lines of Highly Ionized Iron,
Normalized So That the Maximum Observed Flux is 1.00..... 15
3. The Derived Differential Emission Measure Function at Four
Indicated Times (UT) During the Flare..... 24
4. An Illustration of the Effect of Element Abundances on the
Derived Differential Emission Measure Function..... 26

TABLES

1. Selected X-Ray Lines.....	14
2. Flare Parameters.....	29

I. INTRODUCTION

The SOLEX solar X-ray experiment aboard the U. S. Air Force Space Test Program P78-1 satellite consists of two collimated Bragg crystal X-ray spectrometers (Landecker, McKenzie, and Rugge 1979; McKenzie et al. 1980b). The experiment was designed to study solar activity, primarily through observations of individual active regions. Measurements of solar flare spectra have been hampered by the combination of small spectrometer fields of view (20 and 60 arc sec FWHM) and the lack of a real time pointing capability. Nevertheless we have obtained spectra over the 7.8 - 23.0 Å range during the rise phase of a flare on 1979 June 10 (McKenzie et al. 1980a,b) and spectra of the density-sensitive O VII lines for flares on 1980 April 8 and May 9 (Doschek et al. 1981). The present paper is an analysis of a series of 13 X-ray spectra in the 7.8 - 23.0 Å range taken primarily during the decay phase of a flare on 1979 March 31.

A time series of X-ray spectra provides the opportunity to analyze the evolution of the hot coronal plasma during a flare. In contrast to the situation for the 1979 June 10 flare (McKenzie et al. 1980b), for which we obtained spectra only during a relatively long rise phase, for the 1979 March 31 flare we have spectra covering approximately 2100 seconds during part of the rise, the maximum, and decay phase of the event. The X-ray emission peaked during the second spectral scan. While the June 10 flare data showed no major changes in the temperature structure of the plasma during the rise phase, the

March 31 data, as expected, show the flare cooling during the decay phase.

II. THE FLARE DATA

We consider X-ray observations of McMath Plage Region 15918 (active region 1661) on 1979 March 31 between 2321 and 2356 UT. At the start of our observations a flare was in progress. According to data returned by the MONEX LEM (low energy monitor), a full disk viewing proportional counter operating in the range 1-22 keV (0.6 - 12.4 Å) also aboard P78-1 (Landecker, McKenzie, and Rugge 1979), the peak X-ray emission occurred between 2323.2 and 2324.5 UT with higher energy channels peaking earlier. The SOLRAD 11 1-8 Å detector recorded a maximum flux of about 3×10^{-1} erg-cm $^{-2}$ -s $^{-1}$ (X-ray class M3), according to plots published in Solar Geophysical Data (#417, Part I). An H α flare observed in McMath Region 15918 at coordinates S24, E19 started at about 2318 UT, peaked at 2321, and ended after 2400 UT, and was assigned importance 1B by observers at one observatory and 2B at three others (Solar Geophysical Data #416, Part I). The P78-1 tape-recorded observations ended at 2356.2 UT, by which time the X-ray emission had decayed by at least 65% from the peak in all of the spectral lines of highly-ionized iron to be considered below.

The SOLEX spectrometers were scanning at a rate of 31.25 30.2-arc-second steps per second between Bragg angles of 17.4° and 61.7° during the March 31 flare. SOLEX B, collimated to 60" x 60" (FWHM),

used a rubidium acid phthalate crystal (RAP; $2d = 26.12 \text{ \AA}$) to cover the $7.8 - 23.0 \text{ \AA}$ range. SOLEX A, collimated to $20'' \times 20''$ (FWHM), used ammonium dihydrogen phosphate (ADP; $2d = 10.64 \text{ \AA}$) to cover the range $3.2 - 9.4 \text{ \AA}$. The time required to record a complete spectrum was 168.96 s, and each line was sampled only very briefly during this period. Upon reaching one end of a spectral scan, the spectrometer changed direction and scanned toward the other programmed end point. Therefore, the time interval between successive samplings of a given line was not constant. Lines near the scan ends, such as the O VII lines considered below, were sampled twice in rapid succession and then were unobserved for a relatively long period of time. In addition, SOLEX shares the pointing section of the OSO-like P78-1 satellite with the NRL SOLWIND white light coronagraph (Sheeley *et al.* 1980). At intervals of about ten minutes the solar experiments are automatically pointed at sun center so that a SOLWIND exposure of about one minute duration can be made. During the exposure the SOLEX scan is not interrupted, and the result is that about one-fourth of the spectra have gaps in them. Because of the small field of view of SOLEX A and a pointing offset of 28 arc seconds between the two spectrometers, the SOLEX A counting rates were small; hence this spectrometer provided little data to supplement the SOLEX B observations. Consequently we analyze only the SOLEX B spectra here.

Figure 1 shows selected lines, excited at different temperatures, from three spectral scans during the decay of the 1979 March 31 flare. Data are corrected for detector electronics dead time but not

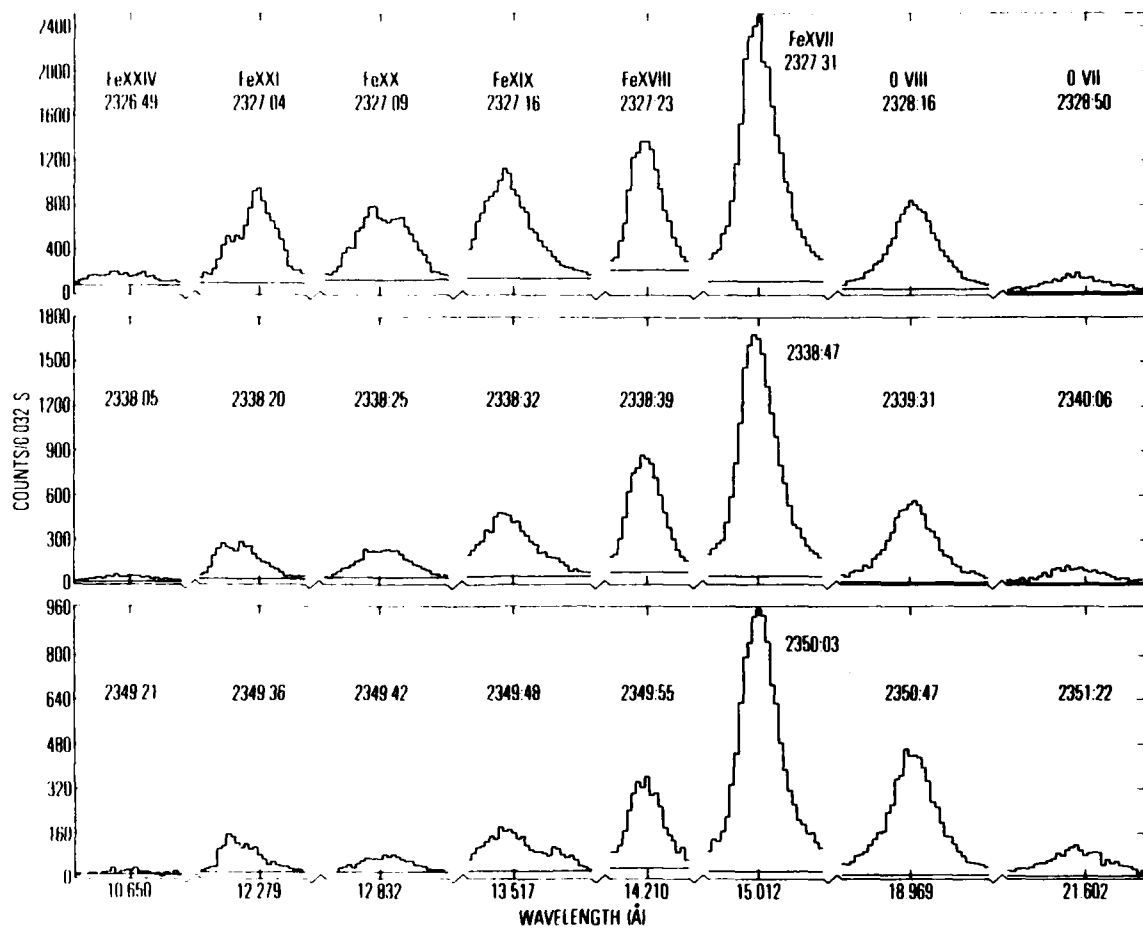


Figure 1: Dead time corrected profiles of selected X-ray lines observed during the 1979 March 31 flare. Each panel displays measurements from one spectral scan with the time at which each line was observed shown above the profile. The horizontal bar beneath each profile is at the local background counting rate level. The lines are identified in Table 1.

instrument response, and the horizontal line beneath each profile is at the background level. The lines and the approximate temperatures at which they are most efficiently produced are shown in Table 1. The plots are scaled so that the highest 32 ms count in the Fe XVII line is nearly full scale. The more rapid decay of the Fe lines from higher stages of ionization makes apparent the cooling of the flare plasma.

III. ANALYSIS

The spectral lines identified in connection with Figure 1 span a wide range of excitation temperatures, and their time-dependent fluxes can be used to describe the cooling of the flare. In Figure 2 the fluxes of a selection of these lines, normalized to the maximum observed flux for each line, are plotted as a function of time. The sample error bars reflect counting statistics only. Systematic uncertainties, especially in estimating the background, could increase the error bars substantially. Each line flux was computed by integrating dead time corrected counts under the line profile and subtracting background. Since each flux is compared only with the same line's flux at a different time, no correction for instrument response was needed in constructing Figure 2. McKenzie *et al.* (1980b) give a detailed description of this data analysis procedure.

Since the Fe XIX lines plotted in the figure are blended with the Ne IX $1s^2$ 1S_0 - $1s2p$ 3P_1 line, a correction had to be made. This was done by using the flux of the Ne IX $1s^2$ 1S_0 - $1s2s$ 3S_1 line at

TABLE I
Selected X-ray Lines

Ion	Transition	Wavelength (Å)	Temperature (10 ⁶ K)	Remarks
O VII	1s ² 1S ₀ - 1s2p 1P ₁	21.60	2	
O VIII	1s ² S _{1/2} - 2p ² P _{1/2, 3/2}	18.97	3	
Fe XVII	2p ⁶ 1S ₀ - 2p ⁵ 3d 1P ₁	15.01	4	
Fe XVIII	2p ⁵ 2P _{3/2} - 2p ⁴ (1D) 3d 2D _{5/2} , 2P _{3/2}	14.21	6	blend
Fe XIX	2p ⁴ 3P ₂ - 2p ³ (2D) 3d 3D ₃ , 3P ₂	13.52	7	blend, also with Ne IX 1s ² 1S ₀ - 1s2p 3P ₁ (see text)
Fe XX	2p ³ 4S _{3/2} - 2p ² (3P) 3d 4P _{5/2, 3/2, 1/2}	12.83	9	blend
Fe XXI	2p ² 3P ₀ - 2p3d 3D ₁	12.28	10	blend with Fe XVII 2p ⁶ 1S ₀ - 2p ⁵ 4d 3D ₁
Fe XXIV	2s ² S _{1/2} - 3p ² P _{3/2, 1/2}	10.64, 10.66	16	partial blend, treated as one line

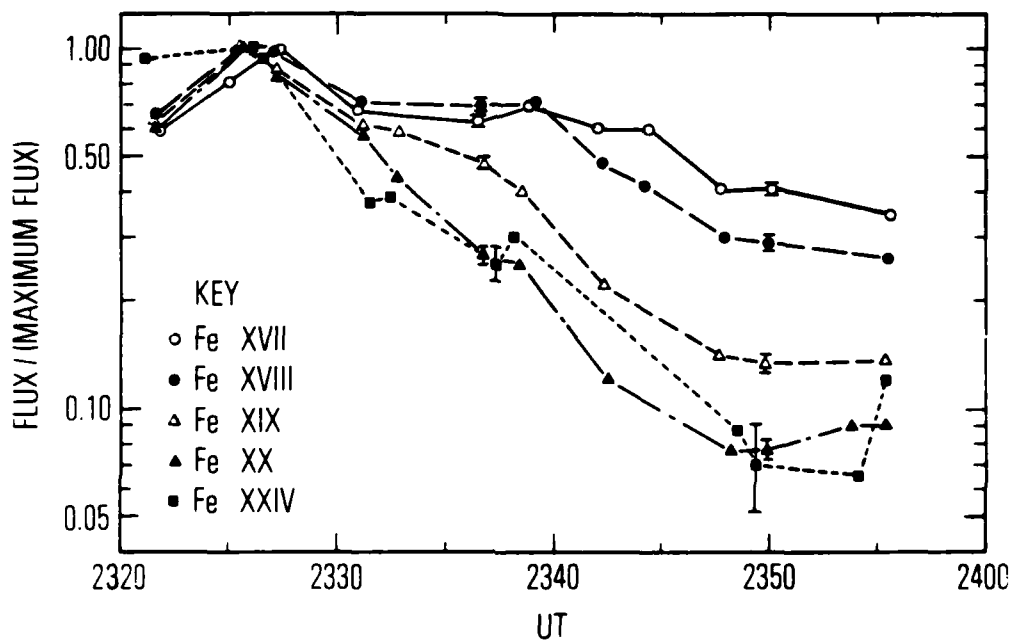


Figure 2: The line flux of selected lines of highly ionized iron, normalized so that the maximum observed flux is 1.00. The measurements are connected to facilitate reading the plots. The lines are identified in Table 1.

13.701 Å. Gabriel and Jordan (1969, 1972) showed that the flux ratio of the 3S_1 to the 3P_1 line is given by

$$R = \left[0.33 \left(1 + \frac{1.35 N_e C (2 ^3S - 2 ^3P)}{A (2 ^3S - 1 ^1S)} \right) \right]^{-1}, \quad (1)$$

where N_e is the electron density. By taking a recently calculated value for the collisional excitation coefficient (Pradhan, Norcross, and Hummer 1981) and $A(2 ^3S - 1 ^1S)$ tabulated by Gabriel and Jordan (1972), we find, for a temperature of 4×10^6 K,

$$R = \frac{3.0}{1 + 1.30 \times 10^{-12} N_e} \quad (2)$$

We do not believe that R for neon varied significantly from its low density limit of 3.0 during this flare. We show below that the maximum observed density for the O VII emitting plasma at 2×10^6 K was $4.7 \times 10^{10} \text{ cm}^{-3}$. Equation (2) shows that a density of $7.7 \times 10^{10} \text{ cm}^{-3}$ at 4×10^6 K would be required for the derived Ne IX 3P_1 flux to be erroneous by 10%. Although such errors cannot be ruled out completely, the corrections to the Fe XIX fluxes were small, ranging from less than 10% before 2342 UT to about 25% for the last plotted measurements. Thus the Fe XIX decay curve would not be significantly affected by errors in the Ne IX 3P_1 flux.

From Figure 2 one sees immediately that the fluxes of all of the plotted lines began to decay within a few minutes of the X-ray flux maximum. Lines from O VII, O VIII, and Fe XXI, not plotted to avoid

severe crowding in the figure, show similar decay curves. O VII lines are emitted at 2×10^6 K, and Fe XXIV lines at about 1.6×10^7 K. Work by Feldman et al. (1980; see also Doschek et al. 1980) has shown that, at least after 2326 UT, very little of the plasma in this flare was at temperatures above 1.8×10^7 K. Thus the fluxes of lines emitted at all temperatures present in the coronal flare began to decrease a short time after the time of maximum X-ray flux.

The simultaneous decay of all the observed emission line fluxes indicates that the flare emission measure, the volume integral over the flare of the square of the electron density ($\int N_e^2 dV$), also began to decrease a short time after flare maximum. This is contrary to results based upon observations made with broad band detectors (Horan 1971) which have the emission measure continuing to increase long after the peak X-ray flux is observed. If we take the time of the X-ray peak to be 2323 UT, at which time the 6 keV X-ray flux measured by the MONEX LEM reached a maximum, observations require that the emission measure began to decrease no more than 500 s after the X-ray peak. Doschek et al. (1980) observed that the emission measure for a number of large flares peaked only a short time after the X-ray flux maximum. Their observations were of lines of Ca XIX and Fe XXV, species present at temperatures above 10^7 K. The present observations extend the result over the entire regime of temperatures in the coronal flare plasma. The apparent error in the broad band results probably lies in the method of analysis. A temperature is deduced from the broad band spectrum and then emission measure is determined by

using this temperature and the absolute flux in a selected energy band. The deduction of temperature is by no means easy, and, since fluxes are often measured at energies substantially higher than kT , a small error in temperature can lead to a large one in emission measure. Effects such as pulse pile-up (Datlowe 1975a) may further complicate the process. The present result is unequivocal: all observed X-ray line fluxes decreased simultaneously so the coronal emission measure must have decreased.

We define the differential emission measure, $\epsilon(T)$, by considering the volume of flare material emitting at temperature T . The total emission measure can be written as $\int N_e^2 \frac{dV}{dT} dT$. We define $\epsilon(T)$ as $N_e^2 \frac{dV}{dT}$. We will use the measured line fluxes to compute $\epsilon(T)$ for the coronal flare plasma. To establish the correctness of the results we will describe in detail the atomic data used and some inflight instrument calibration checks.

The volume emission rate for the spectral line $j \rightarrow i$ at temperature T , arising from collisional excitation from the ground state, is

$$P_{ji} = \frac{8.63 \times 10^{-6} N_e N_g \Omega_{gj} B_{ji} h\nu \exp(-E_{gj}/kT)}{\omega_g \sqrt{T}} \text{ erg cm}^{-3} \text{ s}^{-1} \quad (3)$$

where N_g is the ground state population (cm^{-3}) of the emitting ion, Ω_{gj} is the collision strength from the ground state to state j (averaged over a Maxwellian electron distribution), B_{ji} is the branching ratio, $h\nu$ the X-ray energy, E_{gj} the energy of state j , and ω_g the statistical weight, $2J_g + 1$. If the differential emission measure and

the collision strengths are known, the line fluxes may be computed from equation (3). Conversely, if enough line fluxes and collision strengths are known, the differential emission measure can be estimated.

The difficulty in using equation (3) lies in the scarcity of collision strength data. Collision strengths are difficult to calculate, and, in the X-ray region, few are known. Workers at Los Alamos Scientific Laboratory have compiled calculated collision strength data from a large number of sources (Magee et al. 1977; Merts et al. 1980). The results of calculations of collision strengths between LS terms are given in the form of a convenient fitting formula. Collision strengths for individual J levels are not given. We have used the compiled results for the transitions of O VII, O VIII, Fe XVII, Fe XVIII, Fe XXI, and Fe XXIV shown in Figure 1. Collision strengths for the other lines in Table 1 are unavailable. We discuss the use of these data in the following paragraphs.

The use of the collision strength data is straightforward in the cases of O VII, O VIII, Fe XVII, and Fe XXIV. For O VII and Fe XVII we treat singlet-singlet transitions so the Los Alamos compiled results can be used directly. In addition to collisional excitation from the ground state, cascade from the $2s2p^63d$ 1D_2 level populates the Fe XVII $2s^22p^53d$ 1P_1 level (Louergue and Nussbaumer 1973). The collision strength for the 1D_2 level was taken from Merts et al. (1980). For O VIII the two transitions are completely unresolved, so the entire collision strength is used. For Fe XXIV the two lines are

partially blended, and the numerical analysis is more easily accomplished if they are treated together. The collision strength is in excellent agreement with recent calculations by Hayes (1979).

For Fe XXI the situation is complicated by the fact that the upper term is 3D and the ground term is 3P (the ground state is $2p^2\ ^3P_0$). There are six dipole allowed transitions between the two multiplets. Mason et al. (1979) have calculated collision strengths for Fe XXI individual J levels at energies of 80, 100, and 150 Rydbergs. Their summed LS term to term collision strengths are in excellent agreement with those of Merts et al. (1980). We have used the Merts et al. results because of their convenient form and have apportioned the LS collision strengths among the J transitions in proportion to the Mason et al. 80 Rydberg (1.09 keV) results. 80 Rydbergs is near the threshold energy for the transitions. The branching ratio for the $2p^2\ ^3P_0 - 2p3d\ ^3D_1$ transition, 0.845, was determined from results in Mason et al. Data showing this line and the competing $2p^2\ ^3P_1 - 2p3d\ ^3D_1$ transition at 12.40 Å (McKenzie et al., 1980b) verify that this branching ratio is approximately correct.

The Fe XXI line flux had to be corrected for the contribution of the partially blended Fe XVII $2p^6\ ^1S_0 - 2p^54d\ ^3D_1$ line (12.264 Å; Hutcheon, Pye, and Evans 1976). Figure 1 clearly shows that this blend was quite important late in the flare. The correction was made by determining the $4d\ ^3D_1$ line flux late in the flare, when it dominated the Fe XXI line, and comparing it to the Fe XVII $2p^6\ ^1S_0 - 2p^53d\ ^1P_1$ flux at that time. The ratio of fluxes of the two Fe XVII

lines (0.086) was then used to correct the earlier data. Loulorgue and Nussbaumer (1973, 1975) have shown that this line ratio is only weakly dependent on T provided that $T \geq 5 \times 10^6$ K.

The most difficult problem was with the Fe XVIII blend, $2p^5 2P_{3/2} - 2p^4 (1D) 3d 2D_{5/2}, 2P_{3/2}$ (Feldman *et al.* 1973). The Los Alamos compilation includes LS collision strengths for both transitions but we know of no such calculations for individual J levels. We therefore resorted to the approximation,

$$\Omega_{ij} = \frac{8\pi}{\sqrt{3}} \frac{1}{E_{ij}} \omega_i f_{ij} g, \quad (4)$$

where f_{ij} is the absorption oscillator strength and g the Gaunt factor. Thus, for two transitions having the same E_{ij} and g ,

$$\frac{\Omega_1}{\Omega_2} = \frac{(2J_1 + 1) f_1}{(2J_2 + 1) f_2}, \quad (5)$$

where the J's refer to the lower state of each transition. The Fe XVIII collision strengths were approximated by using the LS collision strengths from the Los Alamos compilation and equation (5) with oscillator strengths computed by Cowan (1973). The branching ratios were derived from transition probabilities computed by Cowan.

The only provision for inflight calibration of the SOLEX spectrometers is a radioactive source that uses alpha particles to generate Mg Ka X-rays (9.9 Å) by fluorescence. From time to time the spectrometers are placed in a special configuration so that the detectors can

be irradiated. These calibration runs have shown that the SOLEX B sensitivity at 9.9 Å has not significantly changed since before launch. In addition, the coronal X-ray spectrum includes a number of line pairs having flux ratios that are only weakly dependent on temperature. By studying these line pairs in active region (nonflaring) spectra, we have been able to verify the SOLEX B calibration.

We have analyzed line pairs from five SOLEX B active region spectra recorded in March and April 1979. The flux ratio of the two O VII lines, $1s^2 \ ^1S_0 - 1s3p \ ^1P_1$ and $1s^2 \ ^1S_0 - 1s2p \ ^1P_1$ at 18.63 Å and 21.60 Å, respectively, depends weakly on temperature. We find an average photon flux ratio of 0.120 ± 0.022 . Rocket flight measurements of an active region by Parkinson (1975) and the quiet corona by McKenzie et al. (1978) found photon ratios of 0.129 and 0.103, respectively. Acton, Catura, and Joki (1975) pointed out that the flux ratio of the O VIII $1s \ ^2S_{1/2} - 2p \ ^2P_{1/2, 3/2}$ line (18.97 Å) to the Ne IX $1s^2 \ ^1S_0 - 1s2p \ ^1P_1$ (13.45 Å) line is only weakly temperature dependent. From 25 rocket observations they obtained a photon flux ratio broadly distributed with an average between 7 and 8. The five SOLEX spectra yield an average ratio of 6.1 ± 0.9 . Parkinson (1975) found 6.8. The ratio of the Fe XVII lines, $2p^6 \ ^1S_0 - 2p^5 3s \ ^1P_1$ at 16.78 Å, and $2p^6 \ ^1S_0 - 2p^5 3d \ ^1P_1$ at 15.01 Å is very weakly temperature dependent, according to Loulorgue and Nussbaumer (1975). They cite data from eight different spectra. The simple average of the energy flux ratio for these measurements is 0.68 ± 0.14 . The five SOLEX active region spectra yield an average energy

flux ratio of 0.69 ± 0.02 . The Fe XVII ratio $2p^6 1s_0 - 2p^5 4d 3D_1$ (12.26 \AA) to $2p^6 1s_0 - 2p^5 3d 1P_1$ (15.01 \AA) is more temperature dependent than the other ratios cited above, but the dependence is weak at temperatures for which Fe XVII lines are strongly emitted. The average photon flux ratio for the SOLEX B measurements was 0.065 ± 0.005 , in good agreement with 0.065 of Parkinson (1975), but well above the values of Hutcheon, Pye, and Evans (1976). Walker, Rugge, and Weiss (1974) find a ratio of 0.061, but they caution that the $4d 3D_1$ line may be blended in their spectra. Taken together, the measurements cited above verify the SOLEX B calibration over a wavelength range including all of the lines studied in this paper except for the Fe XXIV lines at around 10.65 \AA . Since both the detector efficiency and the RAP reflectivity (Burek 1976) are uncomplicated down to the Mg K absorption edge at 9.5 \AA (the detector has a MgF_2 photocathode) we are confident in the calibration above this wavelength.

The differential emission measure was computed with the iterative procedure of Sylwester, Schrijver, and Mewe (1980). In addition to the collision strengths discussed above, we used ionization equilibrium calculations by Jacobs et al. (1977, 1978) and the coronal abundances ($A(\text{Fe}) = 5.25 \times 10^{-5}$, $A(\text{O}) = 4.27 \times 10^{-4}$, $A(\text{H}) = 1$) of Withbroe (1976). $\epsilon(T)$ was constrained to be zero at and above $1.8 \times 10^7 \text{ K}$, in accord with the results of Feldman et al. (1980) for this flare. Figure 3 shows the results. Each curve must be divided by f_c , the collimator transmission averaged over the flaring region. $f_c = 1$ for

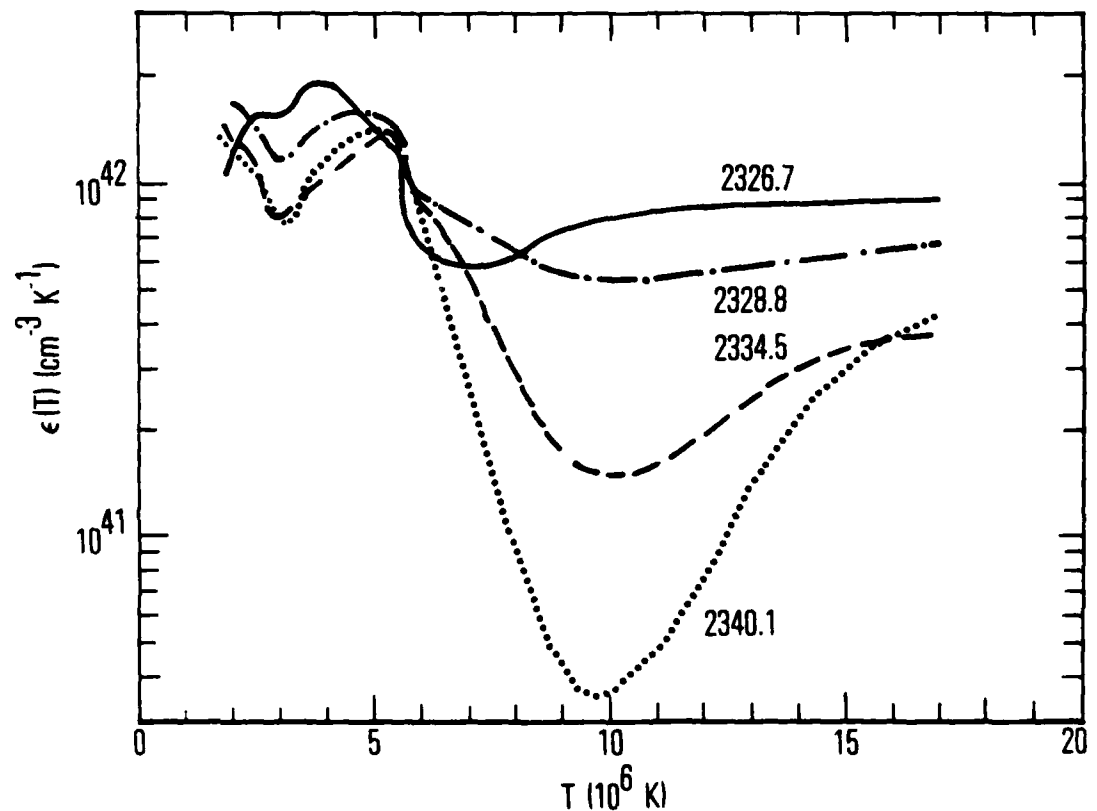


Figure 3: The derived differential emission measure function at four indicated times (UT) during the flare.

a point source on axis, and $f_c = 0.25$ for a flare uniformly filling the collimator field of view. Smaller values occur if the flare is well off-axis. Examination of a raster map of the active region made 82 minutes after the flare peak indicates that the strongest emission was about 10 arc sec off axis at that time. If we assume that this point corresponds to the center of the flare and correct for solar rotation, then the collimator was offset by about 20 arc sec for the flare observations. Based upon this offset and the assumption that the characteristic size of the flare is unlikely to have exceeded 40 arc sec (Landecker and McKenzie 1980), we estimate that f_c^{-1} was in the range 1.50 - 1.75.

At temperatures below 4×10^6 K, $\epsilon(T)$ is uncertain because of uncertainties in the O/Fe abundance ratio. Because the O VIII line has significant emissivity at temperatures as high as 10^7 K, the data summarized in Figure 3 can be used to estimate the O/Fe abundance ratio. We were able to obtain satisfactory fits (i.e., fits that reproduced all line fluxes to within 15%) for $A(O)/A(Fe)$ in the range 5 - 10. Withbroe (1976) lists values of this ratio for the corona ranging from 4.6 to 27 and, in his final tabulation of coronal abundances, $A(O)/A(Fe) = 8.1$. Figure 4 illustrates the uncertainty in $\epsilon(T)$ for one of the spectra. We have plotted the range of $\epsilon(T)$ values, basing the estimated error on the "continuous" error case of Sylwester, Schrijver and Mewe (1980). Two plots are shown, for $A(O)/A(Fe)$ of 5 and 10. The uncertainty introduced by lack of knowledge of the abundances is very large below 4×10^6 K and does not

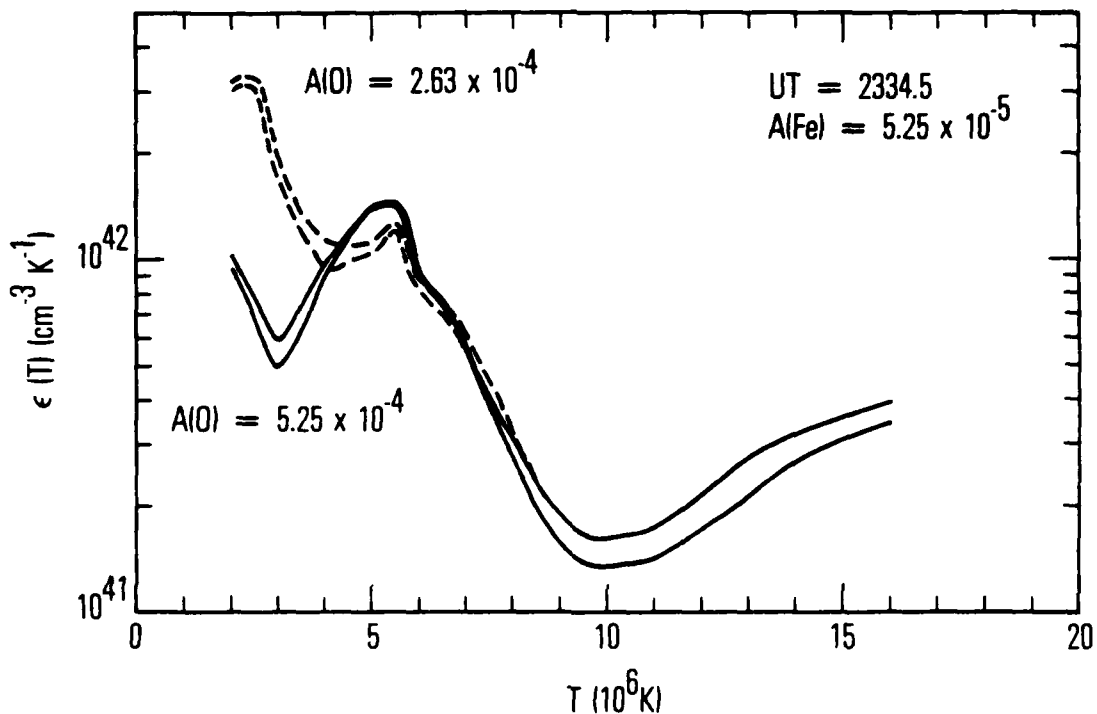


Figure 4: An illustration of the effect of element abundances on the derived differential emission measure function. The range of acceptable values of $\epsilon(T)$ at 2334.5 UT is plotted for two assumptions regarding the O/Fe abundance ratio. As a result of the uncertainty in this ratio, $\epsilon(T)$ is almost unknown for T below $4 \times 10^6 \text{ K}$.

vanish until about 8×10^6 K. We also note that errors in $\epsilon(T)$ confined to a narrow temperature range might be considerably larger than the uncertainties displayed in Figure 4 (Craig and Brown 1976; Sylwester, Schrijver, and Mewe 1980).

The outstanding features of the curves in Figure 3 are the large $\epsilon(T)$ at low and high temperatures and the small $\epsilon(T)$ at around 10^7 K that develop several minutes after the flare peak. The low emission measure at 10^7 K is manifested by low Fe XXI emission. We have verified that this low emission does not result from overcorrecting for the Fe XVII $2p^6 \ 1S_0 - 2p^5 4d \ 3D_1$ line. As noted above, we measured a $(-p^5 4d \ 3D_1)/(2p^5 3d \ 1P_1)$ ratio of 0.086 late in this flare and a ratio of 0.065 in a number of active region spectra. It is not surprising that the ratio is larger in a flare. We have found, however, that the dip in $\epsilon(T)$ also appears if a ratio of 0.065 is used to correct the flare data. With regard to the low temperature $\epsilon(T)$, recall the large uncertainty shown in Figure 4. We cannot say whether $\epsilon(T)$ peaks at around 5×10^6 K or is high at all temperatures below this level.

Figure 3 suggests that $\epsilon(T)$ consists of separate components at high and low temperatures. The material at 10^7 K early in the flare may be part of the low temperature component which cools relatively quickly to reveal a high temperature part with emission measure increasing sharply with increasing temperature. In studies of the energy balance of active regions and the transition zone, Jordan (1976, 1980) cites evidence for $\epsilon(T)$ of the form aT^b for T up to some cut-off

temperature. The hot component appears to be consistent with this form. This would mean that the hot component has very little material below about 10^7 K. Although the cool material shows little change in emission measure during our observations, it should not be thought of as mere background. The O VII, O VIII, and Fe XVII fluxes near the peak of the flare are approximately 10 times those in nonflaring active regions.

By integrating the functions in Figure 3 for T above 2×10^6 K we can determine the emission measure for the entire coronal flare. Most previous work has derived only an apparent emission measure based on an assumed single relatively high temperature for the flare (Datlowe 1975b; Feldman *et al.* 1980). The present method, however, does have the disadvantage that the result must be divided by an uncertain factor f_c . The integrated emission measures are given in Table 2. We also show separately the integral over the hot material below 10^7 K.

The ratio, R , of the $1s^2 \ ^1S_0 - 1s2s \ ^3S_1$ to the $1s^2 \ ^1S_0 - 1s2p \ ^3P_1$ lines of the helium-like ions can be used as an electron density diagnostic (Gabriel and Jordan 1969, 1972). We have measurements of R for OVII and Mg XI. From a previous discussion herein one can see that our Ne IX measurements are unsuitable for this purpose. For O VII we have (similar to Equation (2) above),

$$N_e = 3.5 \times 10^{10} \left(\frac{3.6}{R} - 1 \right) \quad (6)$$

TABLE 2
Flare Parameters

Time (UT)	Unit	2326.7	2328.8	2334.5	2340.1
$\int_{T_c}^{1.8 \times 10^7 \text{ K}} \epsilon(T) dT$	$(10^{48} \text{ cm}^{-3})^*$	15.2 -1.5	+3.2 -2.1	+3.9 -2.1	+2.7 -0.9
$\int_{T_c}^{2 \times 10^6 \text{ K}} \epsilon(T) dT$	$(10^{48} \text{ cm}^{-3})^*$	8.7 -1.3	+3.1 -1.4	+3.3 -1.4	+2.5 -0.7
$N_e (2 \times 10^6 \text{ K})$	$(10^{10} \text{ cm}^{-3})$	---		4.8 ± 0.5	2.8 ± 0.5
$P_e (2 \times 10^6 \text{ K})$	(dyne-cm^{-2})	---		13.3 ± 1.4	7.7 ± 1.4
$f_c P_R$	$(10^{26} \text{ erg-s}^{-1})^*$	8.6 -1.3	+3.8 -1.3	+3.6 -1.5	+2.6 -0.8
					$+2.3$ 4.2 -0.8

*Uncertainty based on $\epsilon(T)$ functions for extreme values of $A(\text{Fe})/A(\text{O})$ (see Figure 4).

This differs from the expression we have previously used (McKenzie *et al.* 1980a) because here we use new collision strength calculations by Pradhan, Norcross, and Hummer (1981). Our earlier derived densities should be reduced by a factor of 1.9 to correspond to the use of these collision strengths. Electron densities, N_e , and pressures, P_e , ($P_e = N_e kT$) for an assumed temperature of 2×10^6 K are given in Table 2. The maximum observed density of 4.8×10^{10} cm $^{-3}$ is lower than the 9×10^{10} cm $^{-3}$ obtained when our 1979 June 10 observations (McKenzie *et al.* 1980a) are corrected by the above-mentioned factor of 1.9, and is much lower than the 10^{12} cm $^{-3}$ found for flares on 1980 April 8 and May 9 (Doschek *et al.* 1981). In the March 31 flare we had no O VII observations until after the peak, and densities may have been considerably higher earlier. The observed rapid decrease in density shows that the cooler coronal material was active in the flare process despite the slow variation in $\epsilon(T)$.

For Mg XI ($T = 6 \times 10^6$ K),

$$N_e = 1.6 \times 10^{13} \left(\frac{2.6}{R} - 1 \right) \quad (7)$$

(Gabriel and Jordan 1972). For 11 scans the mean value of R was 2.31 with a standard deviation of the mean of 0.08. The lowest measured R was 1.97 ± 0.28 , and this was very late in the flare (2354.8 UT). We do not find any positive density determination but set an upper limit of 9×10^{12} cm $^{-3}$ from the above measurement and equation (7).

Observations from Skylab (Vorpahl et al. 1975; Kahler, Krieger, and Vaiana 1975) have shown that the hot flare plasma is located in arches or loops. A pressure equilibrium can establish itself in the time required for sound to travel the length of a loop (Moore et al. 1980). Then a short time after the flare begins to cool the differential emission measure can be expressed as the product $N_e^2(T) \frac{dV}{dT}$; that is, the temperature can be expressed as a function of position along the loop. It is usually assumed (Moore et al. 1980) that the temperature is highest at the top of the loop and the flare cools by radiation and conduction down the loop. The total thermal energy in the loop can be written as

$$E = \frac{3}{2} k \int (N_e + N_I) T dV = 2.8 k \int N_e T dV = 2.8k^2 \int \frac{N_e^2 T^2 dV}{P_e}$$

$$= 2.8k^2 \int \frac{T^2 N_e^2 \frac{dV}{dT} dT}{P_e} , \quad (8)$$

where N_I is the ion density. Equation (8) assumes the helium abundance is 20% of the hydrogen abundance and the ion temperature equals the electron temperature.

If $P_e(T)$ is known the thermal energy can be computed. Unfortunately we know only the average pressure for temperature around 2×10^6 K; i.e., near the bottom of the loops. It would be convenient to assume P_e is a constant. If the loops are in hydrostatic equilibrium, a pressure gradient is required to support the material near the tops. If the weight per unit area of the loop material is small compared to the pressure near the feet, constant P_e may be a good approximation. The weight per unit area, w , is given by

$$w = 1.3 \int \frac{m_H g_s}{A} N_e \frac{dV}{dT} dT = 1.3 m_H g_s k \int \frac{T}{P_e A} N_e^2 \frac{dV}{dT} dT , \quad (9)$$

where m_H is the proton mass, g_s is the gravitational acceleration at the surface of the sun, A is the cross-sectional area of the loop(s), and the integral is over T greater than 2×10^6 K. The multiplying factor 1.3 arises from the choice of helium abundance of 20% of the hydrogen abundance. Checking the above-stated criterion for consistency with the assumption that P_e is constant we require $w \ll P_e$, or

$$A > 1.3 \frac{m_H g_s k}{P_e^2} \int T N_e^2 \frac{dV}{dT} dT , \quad (10)$$

provided that the tubes are not tapered. For the March 31 flare at 2328.8 UT this becomes $A \gg 5 \times 10^{18} \text{ cm}^2$ or $A \gg 3.3 \text{ deg}^2$. The Big Bear Observatory measured the H α flare area at 4.8 deg^2 (Solar Geophysical Data #416, Part I). If we take the H α area as an upper limit on the cross-sectional area of the X-ray loops we see that the criterion in equation (10) is not satisfied; the weight per unit area is not negligible compared to the pressure near the base of the loops. Since T enters the integral of equation (8) in the second power, our ignorance of the pressure at high temperature is particularly unfortunate. Very little information is available on the high temperature flare energetics. Because currently known density-sensitive lines excited at high temperatures only enable very high densities to be determined, it is doubtful that this situation can be

improved in the near future. X-ray or XUV images with very high spatial resolution might allow densities to be deduced, but such images are currently unavailable.

The rate of radiative energy loss, P_R , can be determined easily:

$$P_R = \int \Lambda(T) N_e^2 \frac{dV}{dT} dT \text{ erg/s} . \quad (11)$$

$\Lambda(T)$, the radiative energy loss rate is defined by the equation. Table 2 gives P_R , which was computed using $\Lambda(T)$ from Raymond, Cox, and Smith (1976), corrected for the higher iron abundance we use. A very rough estimate of the energy content can be made by performing the integral in Equation (8) assuming $P_e = \text{constant}$. At 2328.8 UT this gives 5×10^{30} ergs and a radiative decay time of 7×10^3 s. Only if P_e is higher at high T (near the tops of the loops) than at low T , will the radiative decay time be shorter. In this case hydrostatic equilibrium would not obtain. Moore et al. (1980) give a simple expression for the conductive decay time:

$$\tau_c = 4 \times 10^{-10} \frac{L^2 N_e}{T^{5/2}} \text{ s.} \quad (12)$$

If $L = 2 \times 10^9$ cm, a typical value reported by Vorpahl et al. (1975), $N_e = 5 \times 10^{10} \text{ cm}^{-3}$, and $T = 1.8 \times 10^7$ K, $\tau_c = 58$ s. Moore et al. estimate that τ_c might be an order of magnitude larger if the flux tubes are tapered. Although the estimates are quite rough, it appears that conductive cooling played a more important role than radiative cooling in this flare.

IV. SUMMARY

We have obtained 13 X-ray spectra (7.8 - 23.0 Å) during a solar flare on 1979 March 31. The temperature evolution of the hot flare plasma can be seen by examination of this time series of spectra. The differential emission measure function has been derived at four times during the flare decay. The conclusions of the study are summarized in this section.

The fluxes of spectral lines emitted at temperatures from 2×10^6 K to 18×10^6 K, the maximum flare temperature, decreased within 500 s of the time of peak X-ray emission. This demonstrates that the total emission measure also began to decline near the time of flare maximum, contrary to results derived from earlier broad band observations. The differential emission measure had two components, above and below about 10^7 K. The low temperature part had the larger emission measure throughout the flare decay and dropped off rapidly at temperatures above 5×10^6 K. The high temperature component rose steeply with temperature in the range $10-18 \times 10^6$ K and was consistent with the form $\epsilon(T) = aT^b$.

Knowledge of the differential emission measure function enabled us to determine the total emission measure and the radiative energy loss rate from the flare. The electron pressure (or density) could be measured only at a temperature of 2×10^6 K where a ratio of O VII lines is useful. There is currently no satisfactory way to determine densities at temperatures above a few million K. Furthermore, in this

flare at least, there is no justification for the use of the simplifying assumption, $P_e = \text{constant}$. A consequence is that very little information is available on the flare energetics. Despite large uncertainties arising from our ignorance of P_e and of the flare geometry, we conclude that conductive cooling was dominant over radiative cooling in this flare.

REFERENCES

Acton, L. W., Catura, R. C., and Joki, E. G. 1975, Ap. J. (Letters),
195, L93.

Burek, Anthony 1976, Space Sci. Inst., 2, 53.

Cowan, R. D. 1973, unpublished atomic data.

Craig, I. J. D., and Brown, J. C., 1976, Astr. Ap., 49, 239.

Datlowe, D. W. 1975a, Space Sci. Inst., 1, 389.

1975b, Solar Gamma-, X-, and EUV Radiation, I. A. U.
Symp. No. 68, 191.

Doschek, G. A., Feldman, U., Kreplin, R. W., and Cohen, L. 1980, Ap. J., 239, 725.

Doschek, G. A., Feldman, U., Landecker, P. B., and McKenzie, D. L. 1981 Ap. J. (to be published).

Feldman, U., Doschek, G. A., Cowan, R. D., and Cohen, Leonard 1973, J. Opt. Soc. Am., 63, 1445.

Feldman, U., Doschek, G. A., Kreplin, R. W., and Mariska, John T. 1980, Ap. J., 241, 1175.

Gabriel, A. H., and Jordan, Carole 1969, M. N. R. A. S., 145, 241.

1972, in Case Studies in Atomic Collision Physics, Vol 2, ed. E. W. McDaniel and M. R. C. McDowell (Amsterdam, North Holland), p. 209.

Hayes, M. A. 1979, M. N. R. A. S., 189, 55P.

Horan, D. M. 1971, Solar Phys., 21, 188.

Hutcheon, R. J., Pye, J. P., and Evans, K. D. 1976, M. N. R. A. S., 175, 489.

Jacobs, V. L., Davis, J., Kepple, P. C., and Blaha, M. 1977, Ap. J., 211, 605.

Jacobs, V. L., Davis, J., Rogerson, J. E., and Blaha, M. 1978, J. Quant. Spectrosc. Rad. Transf., 19, 591.

Jordan, Carole 1976, Phil. Trans. Roy. Soc. London A, 281, 391.
1980, Astr. Ap., 86, 355.

Kahler, S. W., Krieger, A. S., and Vaiana, G. S. 1975, Ap. J. (Letters), 199, L57.

Landecker, P. B., McKenzie, D. L., and Rugge, H. R. 1979, Proc. S. I. E., 184, 285.

Landecker, P. B. and McKenzie, D. L. 1980, Ap. J. (Letters), 241, L175.

Loulergue, M., and Nussbaumer, H. 1973, Astr. Ap., 24, 209.

Loulergue, M., and Nussbaumer, H. 1975, Astr. Ap., 45, 125.

Magee, N. H., Jr., Mann, J. B., Merts, A. L., and Robb, W. D. 1977, Los Alamos Scientific Laboratory LA-6691-MS.

Mason, H. E., Doschek, G. A., Feldman, U., and Bhatia, A. K. 1979, Astr. Ap., 73, 74.

McKenzie, D. L., Rugge, H. R., Underwood, J. H., and Young, R. M. 1978, Ap. J., 221, 342.

McKenzie, D. L., Broussard, R. M., Landecker, P. B., Rugge, H. R., Young, R. M., Doschek, G. A., and Feldman, U. 1980a, Ap. J. (Letters), 238, L43.

McKenzie, D. L., Landecker, P. B., Broussard, R. M., Rugge, H. R.,
Young, R. M., Feldman, U., and Doschek, G. A. 1980b, Ap. J., 241,
409.

Merts, A. L., Mann, J. B., Robb, W. D., and Magee, N. H., Jr. 1980,
Los Alamos Scientific Laboratory LA-8267-MS.

Moore, R., McKenzie, D. L., Svestka, Z., Widing, K. G., Antiochos, S.
K., Dere, K. P., Dodson-Prince, H. W., Hiei, E., Krall, K. R.,
Krieger, A. S., Mason, H. E., Petrasso, R. D., Pneuman, G. W.,
Silk, J. K., Vorpahl, J. A., and Withbroe, G. L. 1980, in Solar
Flares, ed. P. A. Sturrock (Boulder, Colorado Assoc. Univ.
Press), p. 341 ff.

Parkinson, John H. 1975, Solar Phys., 42, 183.

Pradhan, A. K., Norcross, D. W., and Hummer, D. G. 1981, Ap. J. (in
press).

Raymond, John C., Cox, Donald P., and Smith, Barham W. 1976, Ap. J.,
204, 290.

Sheeley, N. R., Jr., Michels, D. J., Howard, R. A., and Koomen, M. J. 1980,
Ap. J. (Letters), 237, L99.

Solar Geophysical Data, 1979, 416 Pt. I (Boulder, Colorado: U. S.
Department of Commerce), p. 23.

_____, 1979, 417 Pt. I (Boulder, Colorado: U. S.
Department of Commerce), p. 137.

Sylwester, J., Schrijver, J., and Mewe, R. 1980, Solar Phys., 67, 285.

Vorpahl, J. A., Gibson, E. G., Landecker, P. B., McKenzie, D. L., and
Underwood, J. H. 1975, Solar Phys., 45, 199.

Walker, A. B. C., Jr., Rugge, H. R., and Weiss, K. 1974, Ap. J., 194,
471.

Withbroe, G. L. 1976, Center for Astrophysics preprint series, No.
524.

LABORATORY OPERATIONS

The Laboratory Operations of The Aerospace Corporation is conducting experimental and theoretical investigations necessary for the evaluation and application of scientific advances to new military concepts and systems. Versatility and flexibility have been developed to a high degree by the laboratory personnel in dealing with the many problems encountered in the nation's rapidly developing space and missile systems. Expertise in the latest scientific developments is vital to the accomplishment of tasks related to these problems. The laboratories that contribute to this research are:

Aerophysics Laboratory: Launch and reentry aerodynamics, heat transfer, reentry physics, chemical kinetics, structural mechanics, flight dynamics, atmospheric pollution, and high-power gas lasers.

Chemistry and Physics Laboratory: Atmospheric reactions and atmospheric optics, chemical reactions in polluted atmospheres, chemical reactions of excited species in rocket plumes, chemical thermodynamics, plasma and laser-induced reactions, laser chemistry, propulsion chemistry, space vacuum and radiation effects on materials, lubrication and surface phenomena, photo-sensitive materials and sensors, high precision laser ranging, and the application of physics and chemistry to problems of law enforcement and biomedicine.

Electronics Research Laboratory: Electromagnetic theory, devices, and propagation phenomena, including plasma electromagnetics; quantum electronics, lasers, and electro-optics; communication sciences, applied electronics, semiconducting, superconducting, and crystal device physics, optical and acoustical imaging; atmospheric pollution; millimeter wave and far-infrared technology.

Materials Sciences Laboratory: Development of new materials; metal matrix composites and new forms of carbon; test and evaluation of graphite and ceramics in reentry; spacecraft materials and electronic components in nuclear weapons environment; application of fracture mechanics to stress corrosion and fatigue-induced fractures in structural metals.

Space Sciences Laboratory: Atmospheric and ionospheric physics, radiation from the atmosphere, density and composition of the atmosphere, aurorae and airglow; magnetospheric physics, cosmic rays, generation and propagation of plasma waves in the magnetosphere; solar physics, studies of solar magnetic fields; space astronomy, x-ray astronomy; the effects of nuclear explosions, magnetic storms, and solar activity on the earth's atmosphere, ionosphere, and magnetosphere; the effects of optical, electromagnetic, and particulate radiations in space on space systems.

THE AEROSPACE CORPORATION
El Segundo, California

DATE
ILMED
5-8